Dovepress

ORIGINAL RESEARCH

Strategies for Improved pDNA Loading and Protection Using Cationic and Neutral LNPs with Industrial Scalability Potential Using Microfluidic Technology

Ilaria Ottonelli [1,*], Elisa Adani [2,*], Andrea Bighinati [2], Sabrina Cuoghi [1], Giovanni Tosi [1,3], Maria Angela Vandelli [1], Barbara Ruozi [1], Valeria Marigo [2,3], Jason Thomas Duskey [1]

[1]Nanotech Lab, Te.Far.T.I., Department of Life Sciences, University of Modena and Reggio Emilia, Modena, Italy; [2]Department of Life Sciences, University of Modena and Reggio Emilia, Modena, Italy; [3]Center for Neuroscience and Neurotechnology, Modena, Italy

*These authors contributed equally to this work

Correspondence: Jason Thomas Duskey, Nanotech Lab, Te.Far.T.I., Department of Life Sciences, University of Modena and Reggio Emilia, Via Giuseppe Campi 103, Modena, MO, Italy, 41125, Tel +390592058573, Email jtduskey@unimore.it; Valeria Marigo, Department of Life Sciences, University of Modena and Reggio Emilia, Via Giuseppe Campi 287, Modena, MO, 41125, Italy, Tel +390592055392, Email vmarigo@unimore.it

Purpose: In recent years, microfluidic technologies have become mainstream in producing gene therapy nanomedicines (NMeds) following the Covid-19 vaccine; however, extensive optimizations are needed for each NMed type and genetic material. This article strives to improve LNPs for pDNA loading, protection, and delivery, while minimizing toxicity.
Methods: The microfluidic technique was optimized to form cationic or neutral LNPs to load pDNA. Classical "post-formulation" DNA addition vs "pre" addition in the aqueous phase were compared. All formulations were characterized (size, homogeneity, zeta potential, morphology, weight yield, and stability), then tested for loading efficiency, nuclease protection, toxicity, and cell uptake.
Results: Optimized LNPs formulated with DPPC: Chol:DOTAP 1:1:0.1 molar ratio and 10 μg of DOPE-Rhod, had a size of 160 nm and good homogeneity. The chemico-physical characteristics of cationic LNPs worsened when adding 15 μg/mL of pDNA with the "post" method, while maintaining their characteristics up to 100 μg/mL of pDNA with the "pre" addition remaining stable for 30 days. Interestingly, neutral LNPs formulated with the same method loaded up to 50% of the DNA. Both particles could protect the DNA from nucleases even after one month of storage, and low cell toxicity was found up to 40 μg/mL LNPs. Cell uptake occurred within 2 hours for both formulations with the DNA intact in the cytoplasm, outside of the lysosomes.
Conclusion: In this study, the upcoming microfluidic technique was applied to two strategies to generate pDNA-LNPs. Cationic LNPs could load 10x the amount of DNA as the classical approach, while neutral LNPs, which also loaded and protected DNA, showed lower toxicity and good DNA protection. This is a big step forward at minimizing doses and toxicity of LNP-based gene therapy.
Keywords: gene therapy, lipid nanoparticles, microfluidics, lipoplexes, DNA delivery

Introduction

Nanomedicines (NMeds) have been designed to improve half-life, stability, lower necessary doses, offer targeted delivery, and importantly, protect the pharmaceutical molecule.[1–6] This has led to NMeds becoming a major point of interest in the research for new pharmaceutical options in the treatment of almost every major, orphan, and hard to treat disease.[7–13] The advantages of the use of NMeds are even more evident with the advancement of gene therapeutics where the genetic material must be well protected from the immune system, delivered to the site of interest with high specificity, enter into the cell, and arrive at the point of interest (nucleus or cytoplasm) in a sufficient amount for a therapeutic effect.[14–17] In fact, when discussing DNA delivery, and/or its co-delivery with other molecules such as siRNA, great

strides have already, and still are, being made demonstrating these capabilities in a variety of NMed systems ranging from dendrimers,[18–22] inorganic,[23–25] polymeric,[26–31] and lipidic[32–36] nanoparticles which were able to protect, target, and effectively transfect genes in in vitro studies. Cationic charges have been primarily used to stabilize the DNA through charge interaction in order to protect the plasmid DNA being delivered, even though the charge interaction with cell surface proteins was correlated to cell toxicity.[37–40] Recently, research has drifted away from large pDNA towards the use of siRNA and mRNA for their small size, high expression, and ability to knock down or lead to protein expression respectively without having to enter the nucleus; however, they also suffer from easy degradation during formulation and after administration, making their use difficult. While a drawback for pDNA was the requirement of nuclear localization it is recently being reconsidered.[41,42] Its higher stability coupled with the emergence of advanced integrating systems, such as CAS9, which allow integration of pDNA into the genome, thus leading to permanent and high expression of a corrected gene.[43–47]

While research in gene therapy continues to expand rapidly, it still lacks an efficient and scalable method for industrial production. Microfluidic (MF) technology led to the breakthrough allowing the development and global distribution of the COVID-19 vaccine using lipidic mRNA formulations, which has led to a boom in gene therapy-based pharmaceuticals.[48–51] This technique uses automated pump systems to pass solvents containing the drugs and the material to form the NMeds through a MF chip, allowing for NMed formulations with improved output, reproducibility, automation, and the possibility for GMP processing.[52–55] While MF helped to improve formulations, numerous barriers need to be overcome in order to transfer this industrial focused technique to the research and small lab settings in the Universities etc. First of all, the major settings of the microfluidic device for each individual drug and NMed system must be optimized: total flow rate (TFR), flow rate ratio (FRR), total volume, and concentrations of the materials.[56–59] Optimization is also required for MF-NMeds stability, as storage can be problematic for most of the particles produced with this method, as it was for the Comirnaty® vaccine that needed expensive transportation at −80°C.[60] Moreover, some studies indicate that even when the characteristics (size, zeta potential, polydispersity index (PDI), and morphology) appear to be identical to those of the standard benchtop chemistry, the formation of the NMeds is different, leading to variations in both uptake and therapeutic results in vitro and in vivo.[61,62] Therefore, it is necessary to optimize each individual drug and NMed combination in order to ensure consistency when moving into more advanced in vitro or in vivo testing.

This article demonstrates the importance of optimizing MF techniques to produce pDNA-loaded lipidic nanoparticles (LNPs), and not assuming that past literature with classic techniques translate directly. Phospholipids were used to formulate LNPs using a MF chip, to which pDNA was added either to previously formulated liposomes, similar to a traditional benchtop approach, or during the formulation as a solution in the aqueous phase. Both systems were characterized in size, homogeneity, entrapment efficiency, and stability, and tested in vitro. Moreover, a cationic system was compared to a neutral one to assess the actual necessity of the cationic charge during the formulation when using the MF method.

Materials and Methods
Chemicals

1.2-dipalmitoyl-sn-glycero-3-phosphocholine (DPPC) MW 734.039 CAS number 63–89-8, 1.2- dioleoyl-3-trimethylammonium-propane (chloride salt) (DOTAP) MW 698.542 CAS number 132,172–61-3, and 1.2-dioleoyl-sn-glycero-3-phosphoethanolamine-N-(lissamine rhodamine B sulfonyl) (ammonium salt) (DOPE-Rhod) MW 1319.75 CAS number 384,833–00-5 were purchased from Avanti polar lipids (Birmingham-Alabama). Cholesterol (Chol) MW 386.654 CAS number 57–88-5, Methanol (CH3OH) MW 32.04 CAS number 67–56-1 were purchased from Sigma Aldrich (Saint-Louis, Missouri). Agarose, Electrophoresis Grade (C24H38O19) MW 630.55 CAS number 9012–36-6, Sodium dodecyl sulfate MW 288.38 CAS 151–21-3, Ethylenediaminetetraacetic acid (EDTA, Disodium Salt, Dihydrate) MW 372.24 CAS 6381–92-6, Boric acid Electrophoresis Grade (BH3O3) MW 61.83 CAS 10043–35-3, Tris(hydroxymethyl)aminomethane (Tris) MW 121.14 CAS number 77–86-1, SYBR™ Green I nucleic acid gel stain CAS number 163,795–75-3, TriTrack DNA loading dye (6X) were purchased from Thermo Fisher Scientific (Waltham, Massachusetts). The pDNA (pcDNA3-EGFP 6159 bp) was purchased

from Addgene (Watertown, Massachusetts) and contains the eGFP (enhanced Green Fluorescent Protein) cDNA under the control of a CMV (cytomegalovirus) promoter and an SV40 origin of replication in mammalian cells expressing the SV40 large T antigen. A MilliQ water system (Merck Millipore), supplied with deionised water, provided high-purity water (18 MΩ).

LNP Formulation
Formulation of LNPs
LNPs were formulated by using a 3D-printed polypropylene microfluidic chip that was manufactured and kindly donated by Prof. Tiboni. The device has a "split and recombine" design with microchannels having a mean internal diameter of 500 μm,[63,64] and a syringe pump was used to control the flow of the aqueous and organic solutions (IPS-14, Inovenso, Boston, MA, USA). A total of 5 mg/mL of lipid mixture was solubilized in methanol and injected in the microfluidic chip against TE buffer (Tris.HCl 10 mM, EDTA 1 mM pH 8.0 in DNAse free dH₂O), using a total flow rate (TFR) of 10 mL/min and a Flow Rate Ratio (FRR) of 1:1. These conditions were found suitable during previous optimizations of the formulative parameters, where the FRR was varied (1:1:, 1:0.5, 1:0.3) along with the DPPC:Chol ratio (1:0.1, 1:0.5, 1:1, 1:2). Cationic liposomes (DPPC:Chol:DOTAP) have been formulated varying the molar ratio between lipids (1:1:0.01, 1:1:0.05, 1:1:0.1 and 1:1:0.5), with an increasing amount of DOPE-Rhod added to the organic phase. DOPE-Rhod was added at a molar ratio of DPPC:Chol:DOTAP:DOPE-Rhod of 1:1:0.1:0.001, 1:1:0.1:0.005, and 1:1:0.1:0.01, corresponding to 10, 50, and 100 μg per formulation respectively. For better clarity, the mass will be used hereafter referring to the DOPE-Rhod amount. After mixing, the formulations were collected in large beakers and methanol was evaporated for 3–4 hours under magnetic stirring at room temperature (RT) at 500 rpm until 1 mL of final formulation was obtained. Samples were stored at 4°C for further use and utilized within 24 h unless specified.

Plasmid Loaded LNPs
LNPs loaded with plasmid were formulated comparing two different methods: addition post formulation, hereafter referred to as "post", or loading during formulation, referred to as "pre".

In the first strategy, empty liposomes were formulated as previously described and divided into 195 μL aliquots. To these samples, 5 μL of pDNA solution in TE buffer at different concentrations were added under magnetic stirring (1.5 h RT), to obtain different final concentrations of pDNA per sample ranging 5–15 μg/mL.

For the "pre" LNP formulations, the plasmid was diluted in TE buffer pH 8.0, obtaining different concentrations from 5 to 100 μg/mL, and these solutions were used as an aqueous phase during production of the LNPs.

Characterization of the LNPs
Weight Yield % (WY%)
The weight yield (WY) was calculated by placing 500 μL of formulation in a pre-weighed tube and lyophilized for at least 8 h or until completely dry. The weight obtained was compared to the initial amount of lipids used to prepare the formulation, using the following equation:

$$WY\% = \frac{\text{mg lipids expected} - \text{mg lyophilized powder}}{\text{mg lipids expected}} * 100$$

Size, PDI, and Zeta Potential Analysis
The size and polydispersity index (PDI) were measured using a Dynamic Light Scattering (DLS) Zetasizer Nano-ZS (Malvern, Malvern-United Kingdom) at 25°C. The zeta potential was determined using the DTS1070 zeta potential cuvettes (Malvern) using the same instrument. For these analyses, samples were diluted with MilliQ water to obtain a concentration of about 0.2 mg/mL and each measurement was performed in triplicate on three independent formulations.

Dimensional Stability
Dimensional stability to storage stability of the LNPs was evaluated after storage at 4°C. Size, PDI, and zeta potential were tested after either one week (t7) or one month (t30), and the results were then compared to the fresh formulation (t0).

Morphology

The samples were analyzed by using an atomic force microscope (AFM, Park Instruments, Sunnyvale, CA, USA) at about 25°C, operating in air and in non-contact mode, using a commercial silicon tip-cantilever (Zelenograd, Moscow, Russia) with a stiffness of about 40 Nm^{-1} and a resonance frequency around 150 kHz. The sample was diluted in distilled water at 0.01 mg/mL before being applied on a freshly cleaved mica disk; the excess water was removed using a blotting paper and left to dry almost completely to allow the LNPs to attach to the mica surface without further processing. The AFM images were obtained with a scan rate of 1 Hz. Images were processed using ProScan Data Acquisition software.

Samples were also analyzed by scanning transmission electron microscopy (STEM FEI Nova NanoSEM 450, Bruker, Billerica, MA, USA). Briefly, a drop of the same water-diluted suspension (0.01 mg/mL) used for AFM imaging was placed on a 200–mesh copper grid (TABB Laboratories Equipment, Berks, UK), allowed to adsorb, and the suspension surplus was removed by filter paper. All grids were analyzed using the transmission electron microscope operating at 25 kV using a STEM II detector in Field free mode.

Fluorimetry

To select the amount of DOPE-Rhod to use in further experiments, fluorescence intensity of the LNPs was measured using a Jasco Spectrofluorometer FP-8200 (560 nm excitation and 583 nm emission). LNPs were analyzed after diluting 1:250 with MilliQ water to simulate a hypothetical concentration to be used for in vitro tests, and using the same formulations without DOPE-Rhod as a blank. Samples were analyzed as triplicates of three independent formulations.

Plasmid Binding Efficiency

Gel Retardation Assay

Gel electrophoresis (gel retardation assay) was performed to quantify the pDNA complexed with the LNPs in a 0.8% agarose gel in TBE buffer 1x (Tris 89 mM, Boric Acid 89 mM, EDTA 2 mM). DNA-LNPs were loaded into the wells in TriTrack loading dye to track the electrophoresis run, and SYBR green was used as an intercalator to track DNA. After a run at 150V for 1.5 h, LNPs would be retained in the wells with the bound DNA, while the free DNA fraction would move towards the anode and be visible at the corresponding band on the agarose gel. The free DNA was quantified and used to calculate the amount of bound DNA. The transilluminator (Molecular Imager® Gel Doc™ XR+ with Image Lab™ Software, Bio-Rad) was used to visualize the migration of genetic material. Fiji ImageJ was used for band quantification using the dedicated "Analyze Gels" tool. Percentage of bound DNA was calculated as follows:

$$\text{Bound DNA\%} = \frac{(\mu\text{g fed pDNA} - \mu\text{g free pDNA})}{\mu\text{g fed pDNA}} * 100$$

DNase I Assay

To assess the DNA protection ability of LNPs, we developed an assay based on DNase I treatment. Cationic or neutral LNPs containing 300 ng or 500 ng of pDNA or naked pDNA at the same amounts were incubated with 1 U/μL DNase I (MO303, New England Biolabs, Ipswich, Massachusetts) or water for 10 minutes at 37°C. The reaction was blocked by adding 5 mM EDTA and incubating for 10 minutes at 75 °C. Subsequently, DNA was extracted from the LNPs in 1% Triton-X 100 and purified by adding an equal volume of phenol/chloroform solution (P4557, Sigma-Aldrich). After emulsification, samples were centrifuged for 2 minutes at 16,200*g. The aqueous upper phase was transferred into another tube and DNA precipitated in 0.3 M Potassium acetate and 70% cold Ethanol. Samples were incubated overnight at −20°C, then centrifuged for 10 minutes at 16,200*g and 4°C. DNA pellets were washed with absolute Ethanol air dried and finally resuspended in water.

For quantification, all samples with purified pDNA were digested for 1 h at 37 °C with *Hind*III restriction enzyme (R0104, New England Biolab) and run on a 1% agarose gel. The internal standard curve was based on 3 concentrations of naked pDNA similarly digested and loaded into each gel. Bands were quantified using the Image Lab software (Bio-Rad).

In vitro Studies

Cell Culture

Induction capacity of LNPs was evaluated in COS-7, a African green monkey kidney fibroblast-like cell line expressing SV40 T Ag (ATCC: CRL-1651). The uptake of LNPs was assessed in the retinal cell-line ARPE-19, a spontaneously arising human retinal pigment epithelium cell line with normal karyotype (ATCC: CRL-2302[TM]).[65] Materials for cell culture were purchased from Thermo Fisher Scientific. ARPE-19 cells were cultured in Dulbecco's Modified Eagle Medium/Nutrient Mixture F-12 (DMEM/F-12, 31,331,028) supplemented with 10% Fetal Bovine Serum (FBS, 10,270,106), 100 U/mL penicillin and 100 μg/mL streptomycin (15,140,148), COS-7 were cultured in DMEM with 4.5 (11,960) or 1 g/L (22,320) glucose, supplemented with 100 U/mL penicillin and 100 μg/mL streptomycin. Cells were allowed to grow in an incubator at 5% CO_2 and 37°C.

Cell Viability Assay

Cell viability was determined in ARPE-19 cells by the colorimetric methyl-thiazolyl diphenyl-tetrazolium bromide (MTT) assay to assess toxicity of the LNPs. For that, cells were cultured in 96-well plates at a density of 5,000 cells/well and increasing dilutions of LNPs were added to the culture medium. After 48h or 72h, the medium was aspirated and the cells in each well were incubated for 3 h at 37°C with 50 μL of 1 mg/mL MTT solution diluted in the culture medium. The supernatant was removed, the purple formazan crystals were dissolved in 100 μL of isopropanol, and the absorbance was measured at 560 nm using the GloMax Discover microplate reader (Promega, Madison, Wisconsin).

Cell Uptake and Expression Studies

For uptake studies, ARPE-19 cells were seeded onto glass coverslips in a 24-well plate at a density of 50,000 cells/well in complete cell culture medium. The following day, the medium was replaced with serum-free culture medium with 8 μg/mL LNPs and at different times were analyzed by immunofluorescence. For expression studies, COS-7 cells were seeded in a 24-well plate at a density of 20,000 cells/well. The following day, the medium was replaced with culture medium containing 130 μg/mL LNPs (1 μg total DNA). Cells were imaged with the EVOS M5000 Imaging System (Invitrogen).

Immunofluorescence Staining

After incubation with the LNPs, the cells were fixed with 2% paraformaldehyde for 10 min, washed 3 times with phosphate-buffered saline (PBS), blocked and permeabilized 1 h with BSA 3% and Tween 20 0.1% in PBS. Samples were incubated overnight at 4°C with the following primary antibodies: anti-Caveolin-1 (NB100-615, Novus Biological), anti-EEA1 (BD bioscience) diluted 1:100 or Anti-LAMP2 H4A3 (Developmental Hybridoma, USA) diluted 1:2 in blocking solution. After three washes with PBS, the cells were incubated with the AlexaFluor488 goat anti-mouse secondary antibody (Invitrogen) diluted 1:500 and 0.1 μg/mL DAPI for 1 h at room temperature. Slides were mounted with Mowiol 4–88 and images were acquired with the Leica TCS SP8 confocal microscope (Leica, Wetzlar, Germany). Mean fluorescence intensity of LNPs was analyzed in 10 fields with at least 100 cells using the ImageJ software.

PCR on pDNA Extracted from Cells

Cells were incubated for 8 h or 24 h with either cationic LNPs loaded with 100 μg/mL pDNA or neutral LNPs loaded with 30 μg/mL pDNA. Subsequently, the cells were lysed in lysis buffer (NaCl 100 mM, EDTA 25 mM, TrisHCl pH 8 10 mM, SDS 0.5%, Proteinase K 10 ng/mL) for 12 h at 50 °C, shaking at 350 rpm (Thermomixer compact, Eppendorf, Hamburg, Germany). The pDNA was extracted from cells using a phenol/chloroform solution, as described above. Finally, DNA was quantified using a Nanophotometer (NP80, Implen, Munich, Germany) and 100 ng of pDNA were used for PCR amplification of a 728 bp long region of the pDNA. PCR was performed with the following primers: F:5'-TCTATGGTGAGCAAGGGCGAG-3' and R:5'-GCTCTAGATCACCTGTACAGCTCGTCCATGC-3'; using GoTaq[®] Polymerase (M3001, Promega, Madison, Wisconsin) following the manufacturer's protocol. Nucleic acids extracted from a culture well without cells and incubated with LNPs were used as negative control, and the supernatant containing LNPs with pDNA was used as positive control.

Statistical Analysis

Statistical analysis was performed using the software GraphPad Prism 6 (GraphPad Holdings, San Diego, CA, USA). Student's *t*-test was used for LNPs characterization. One-way ANOVA test with Tukey multiple comparison or Two-way ANOVA with Fisher's LSD test were used for in vitro toxicity and uptake, respectively.

Biological replicates were n > 3, the error bars in graphs indicate the standard deviation (SD) from the average and significance was considered as * p < 0.5, ** p < 0.01, *** p < 0.001, and **** p < 0.0001.

Results
Optimization of Empty LNPs

To formulate cationic LNPs for pDNA delivery, a preliminary study about the FRR to be used and the lipidic composition was conducted (Figure S1). First, the DPPC:Chol ratio was tested ranging from 1:0.1 to 1:2, evidencing that the more cholesterol was included in the formulation, the smaller the LNPs, independent from the FRR used (1:1, 1:0.5, 1:0.3). The DPPC:Chol ratio of 1:1 was chosen for further studies, as LNPs showed a size around 150 nm with PDI < 0.2, and the FRR of 1:1 was selected as no significant variations were observed among the FRR tested. DPPC:Chol 1:1 molar ratio LNPs were then formed with the addition of the cationic lipid DOTAP at molar ratios of 0.05, 0.1, and 0.5, also evaluating the effect that the TE buffer might have on the formation of the LNPs. Data showed no differences in size or PDI between using MilliQ water or the TE buffer, although the Zeta potential was reduced from around 40 mV to around 20 mV, as expected due to the presence of the buffer that might mask the surface charge of the LNPs. For in vitro studies, where we had to track the LNPs, a fluorescently labeled lipid (DOPE-Rhod) was added at 0, 10, 50, and 100 μg per formulation. All formulations were tested for their physico-chemical characteristics, trying to maximize fluorescent signal and cationic surface charge, while reducing aggregation and polydispersity. The increase of DOTAP across all concentrations in the absence of DOPE-Rhod did not appear to negatively affect the formation or the yield of the LNPs, with all being approximately 100–130 nm with a PDI < 0.1, having a surface charge that increases from +18 to +30 mV proportional to the amount of DOTAP, and allowing for a recovery of ~70% of product (Figure 1A and Table S1). Nevertheless, a general increase of both size and PDI was observed to be proportional to the amount of DOPE-Rhod added, leading to larger LNPs (> 300 nm) with PDI increasing > 0.2 when adding 50 or 100 μg of DOPE-Rhod. While some of these LNPs were still borderline within the acceptable range of 300 nm and PDI < 0.3, we considered that to have better biodistribution properties in future in vivo delivery approaches, it is preferable to maintain a lower PDI and size. At the same time, the fluorescence intensity was quantified for each formulation and found that increasing the DOPE-Rhod only led to increased fluorescence up to 50 μg, with 100 μg not increasing proportionally (Figure 1B). This
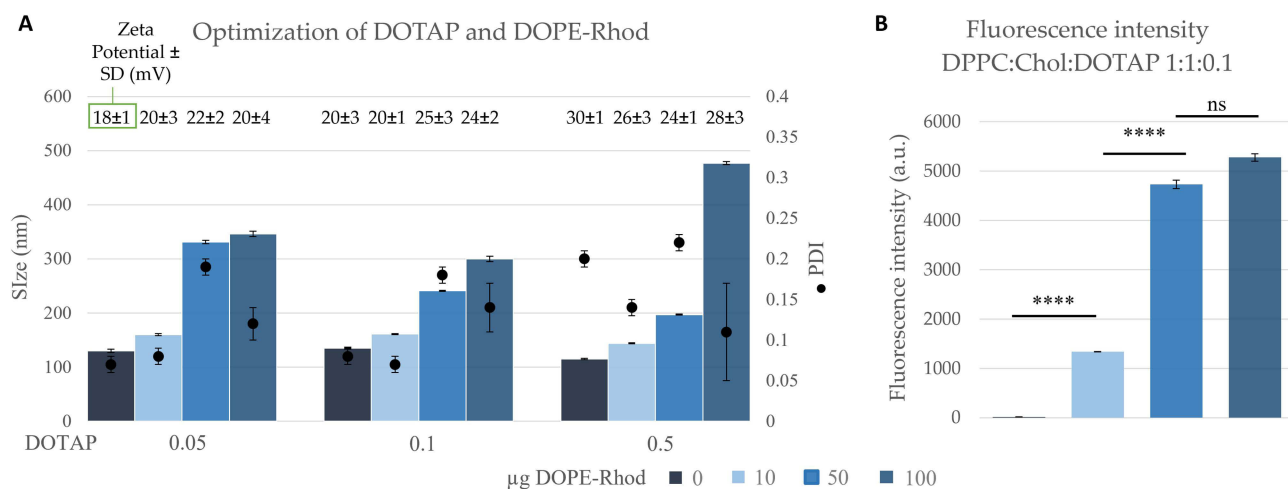
Figure 1 Optimization of the composition of empty LNPs. (**A**) Size, PDI, and Zeta Potential of LNPs with DPPC:Chol:DOTAP 1:1:x molar ratio, and different amounts of DOPE-Rhod. (**B**) Fluorescence intensity of LNPs DPPC:Chol:DOTAP 1:1:0.1 with different amounts of DOPE-Rhod. All samples were analyzed in triplicate, data represent Mean ± SD. ****p < 0.0001, ns = non significant.

minimal increase in fluorescence, along with the worsening of the physico-chemical properties, led to the selection of the LNPs with a composition of DPPC:Chol:DOTAP 1:1:0.1 and 10 µg of DOPE-Rhod for further studies. In fact, this formulation showed sufficient fluorescence intensity and minor differences compared to the non-fluorescent LNPs, while also having the highest amount of cationic lipid. AFM microscopy confirmed that particles had a size of 150–200 nm (Figure S2). The slightly larger size of LNPs measured by AFM was expected due to the drying step and the following "flattening" of the particles on the mica surface during sample preparation, as also reported in the literature.[66–68]

Formulation of pDNA-LNPs

After the optimization of the core structure of the LNPs, the loading and protection of pDNA was tested. Two strategies of adding the DNA were evaluated: 1) addition as a solution post formulation of empty LNPs, hereafter referred to as "post" where the negatively charged DNA interacts with the NMed surface due to charge interaction with the cationic DOTAP, and 2) addition directly into the aqueous phase during formulation, referred to as "pre" where both charge interaction during formulation and encapsulation are possible phenomena (Figure 2).

Post-addition of pDNA on previously formulated empty LNPs was tested with the amount of pDNA ranging 5–15 µg/mL. From the physico-chemical point of view, the addition of pDNA led to a linear increase in size and PDI increasing from ~150 nm and PDI 0.1 to non-homogeneous larger LNPs (250 nm) with PDI > 0.4 (Figure 3, Top), with no variations in the total recovery (Table S2). In all cases ~100% of the DNA was successfully complexed with the cationic LNPs, as shown by a band shift assay (Figure 3, Bottom). However, a huge limitation had to be accounted for because, even if the DNA completely interacted with the LNPs, its addition to previously formed LNPs created a destabilization of the system such that it could not be considered for further analysis.

Contrary to the post-addition LNPs, "pre" added DNA did not lead to an increase in size or PDI up to 15 µg/mL of pDNA, with all LNPs size of ~150 nm and PDI ~ 0.1, and loading 100% of the added pDNA (Figure 3). Based on these positive results, we assessed how much more DNA could be added without negatively affecting the formulation characteristics. A trend towards larger and less monodisperse nanoparticles was observed when we tested up to 100
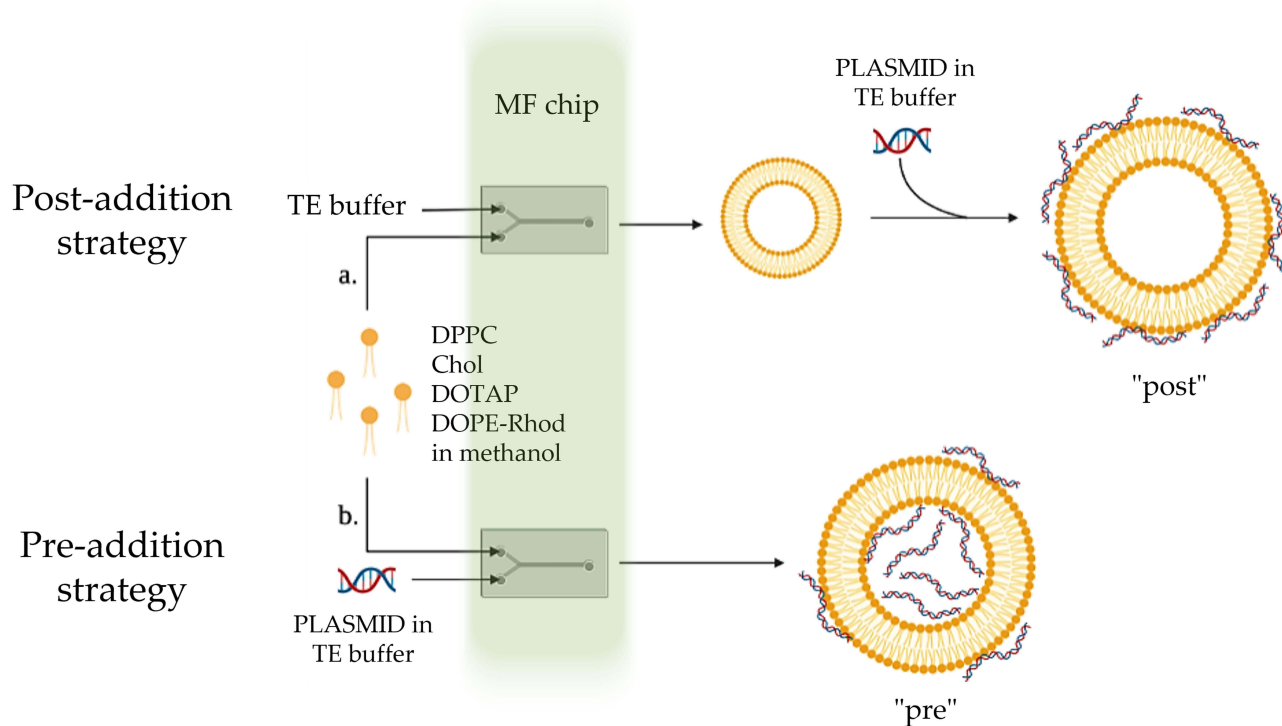
Figure 2 Schematic representation of the two strategies used to formulate pDNA-LNPs using the microfluidic (MF) chip.
Notes: The structure depicted is a simplification of the true structure of the LNPs to better visualize the two formulative approaches.
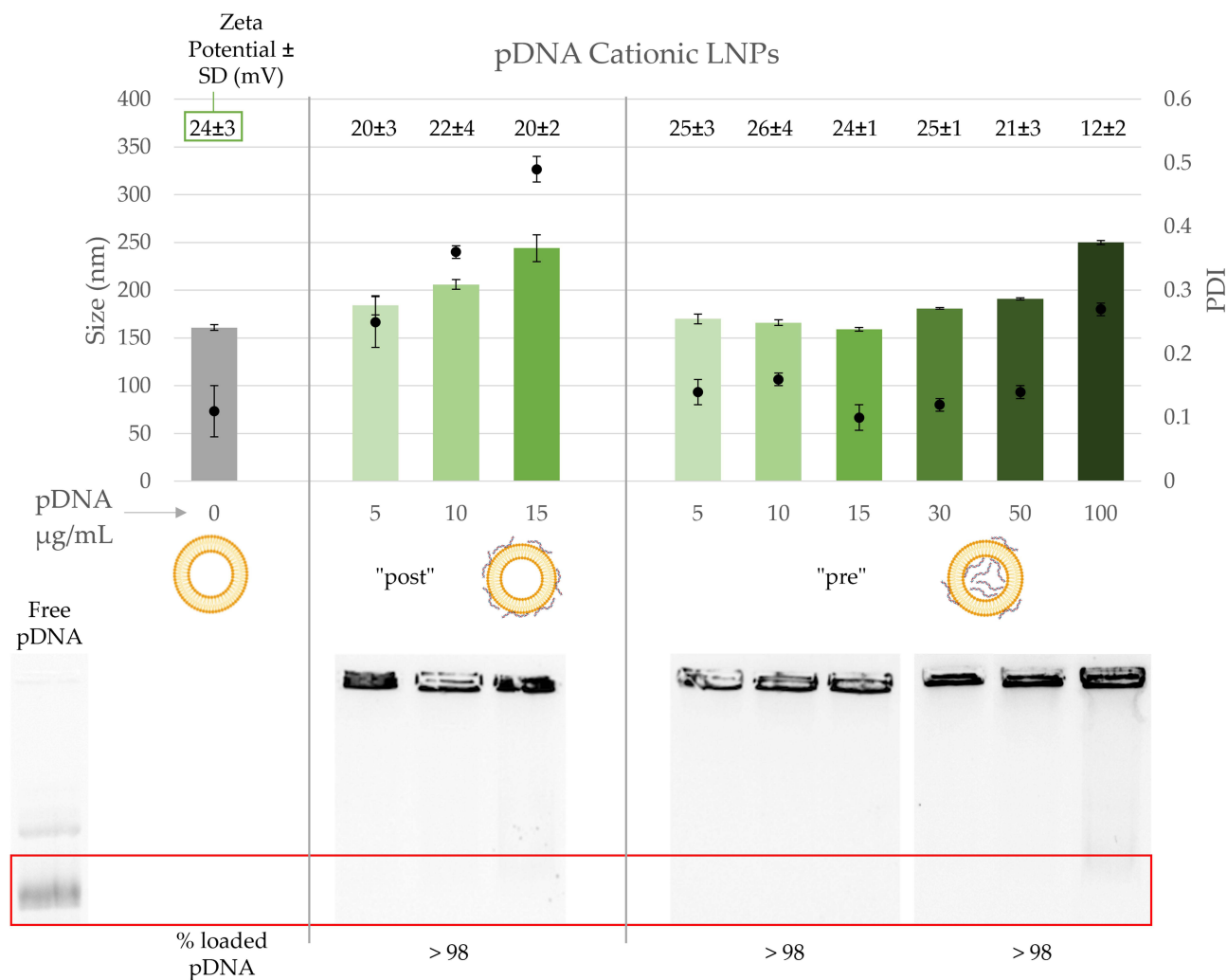
Figure 3 Characterization of cationic pDNA-LNPs. Physical characterization of cationic LNPs empty, post, and pre modified with 0–100 µg/mL of DNA (Top), and their ability to complex the pDNA viewed by band shift assay (Bottom). The red square identifies the area of migration of free pDNA, as showed by the free pDNA run on the left. Percentage of loaded pDNA is reported below based on quantification of the DNA visualized in the gel.

µg/mL, but particles loaded with the highest amount of pDNA were still around 250 nm with PDI < 0.3. This was also matched by a decrease of zeta potential from 25 to 12 mV, most likely due to charge neutralization of the cationic lipid DOTAP by the negatively charged pDNA. Interestingly, the physico-chemical properties and pDNA binding of "pre" 100 µg/mL pDNA-LNPs were maintained after 30 days of storage at 4°C, as confirmed by DLS analysis and gel retardation assay (Figure S3), and AFM microscopy, where round LNPs sized 200–300 nm could be detected both in the fresh sample (Figure 4A) and after 30 days of storage (Figure 4B).

Due to these very positive and interesting results, we evaluated what other beneficial effects the MF technique could offer on pDNA loaded LNPs and focused on the cationic lipid DOTAP added into the formulation. Cationic lipids are added to interact with the DNA by charge interaction as it has long been known that neutral and negative NPs show poor DNA interaction. We confirmed this by testing natural LNPs consisting of only DPPC:Chol 1:1 with the post-addition method. The LNPs showed no difference in physical chemical characteristics, but, as expected, almost no pDNA could be loaded (<5% bound) (Figure 5, bottom left).

Interestingly, "pre" pDNA addition during the formulation of neutral LNPs led to pDNA loaded LNPs, without altering the chemico-physical properties of the particles, which maintained a size around 150 nm with a very narrow distribution (PDI < 0.15) (Figure 5, top right). Addition of pDNA ranging from 0 to 100 µg/mL during the formulation of neutral LNPs showed DNA loading up to 50% of the fed pDNA (Figure 5, bottom), with no significant variations in the
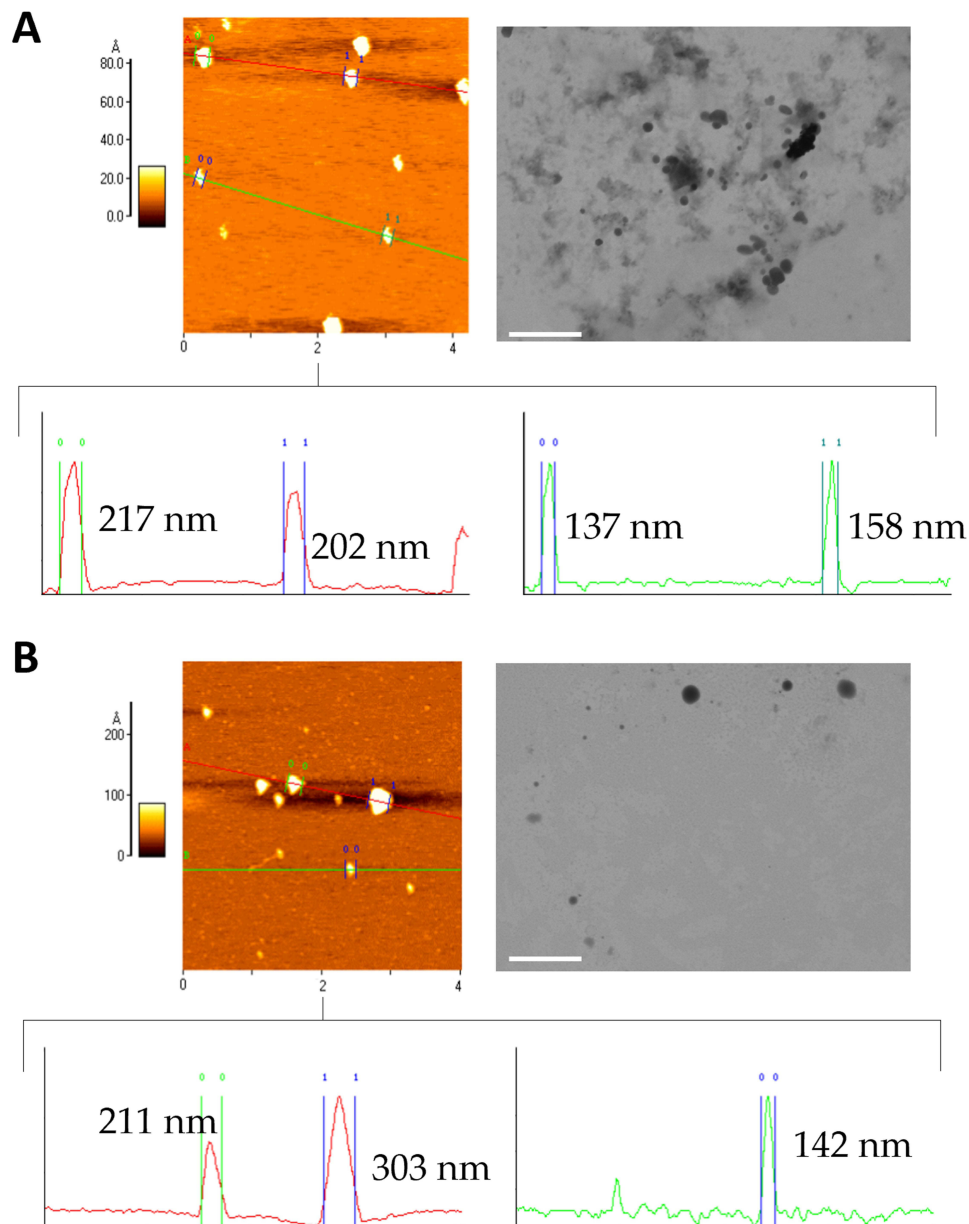
Figure 4 AFM (Topography) and SEM-FEG images of LNPs loaded with 100 μg/mL of plasmid with the «pre» method, as (**A**) fresh formulation, and (**B**) after 1 month of storage at 4°C. Profile analysis of AFM images is reported in the panel below each image. Scale bar: 1 μm.

Zeta potential (around −10 mV), nor in the weight yield (around 70%, Table S3). Due to these improved results, the pre-addition method was selected for all further characterization studies of cationic and neutral LNPs.

DNA Protection Ability

To estimate the amount of pDNA that could be efficiently delivered by the LNPs, and thus evaluate the protection ability of "pre" pDNA-LNPs, pDNA-LNPs were incubated with DNase I and protected nucleic acids were, subsequently, extracted and quantified by gel electrophoresis. On average, the DNA recovered from LNPs after DNase I treatment compared to untreated particles was around 60% and 90% for LNPs loaded with 100 μg/mL or 50 μg/mL pDNA, respectively (Figure 6A). In addition, preservation of the LNP-bound DNA was confirmed by DNase I digestion assay of 100 μg/mL pDNA-LNPs stored for 1 month that behaved similarly to the fresh ones (Figure 6B). These data indicate that
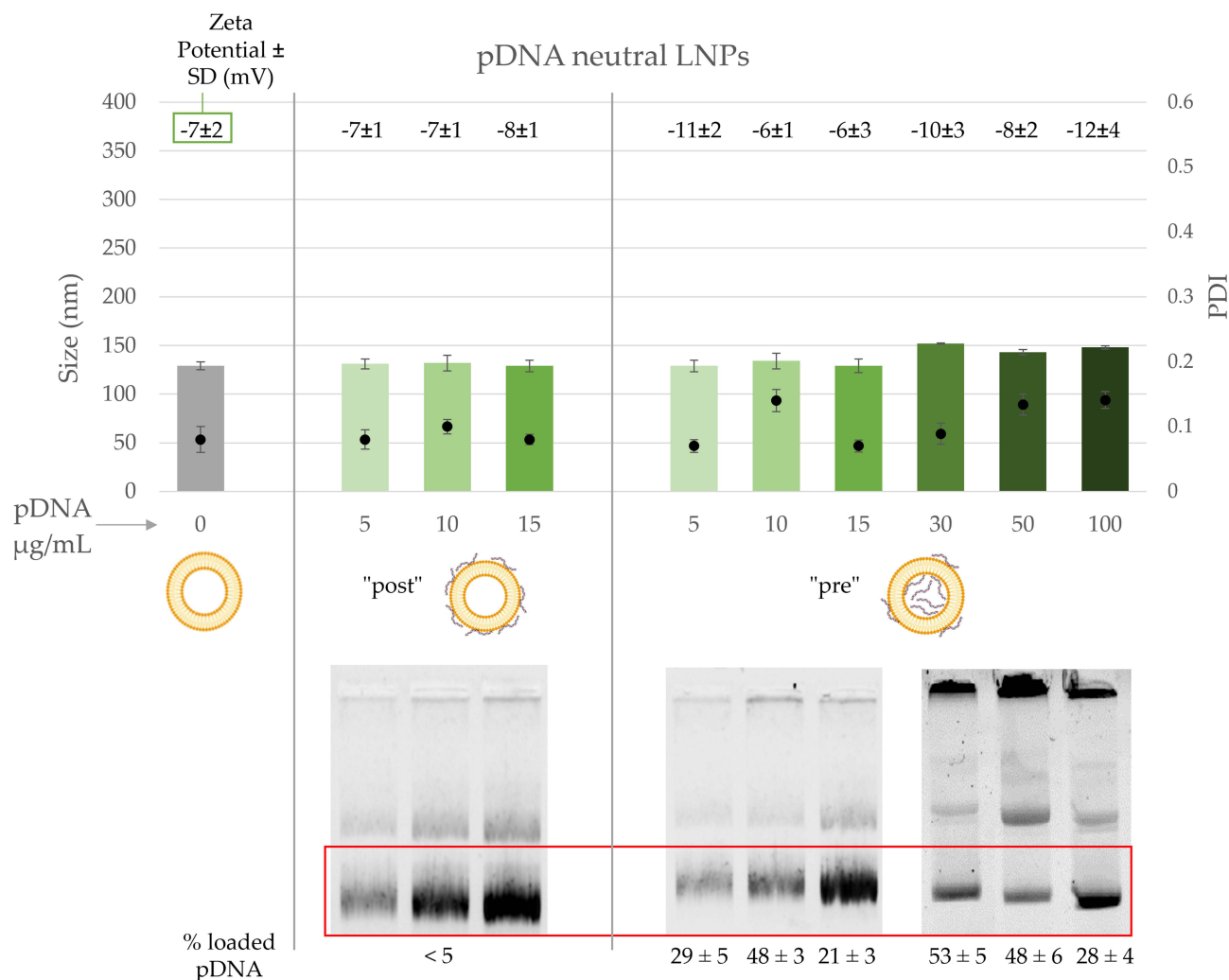
Figure 5 Characterization of neutral pDNA-LNPs. Physical Characterization of neutral LNPs empty, post, and pre modified with 0–100 μg/mL of DNA (Top), and their ability to complex the pDNA viewed by band shift assay (Bottom). The red square identifies the area of migration of free pDNA. Percentage of loaded pDNA is reported below based on quantification of the DNA visualized in the gel.

not only the chemico-physical properties and binding efficiency of these particles were maintained during storage but also that the structural conformation was not significantly altered.

The DNase I protection assay suggested that LNPs formulated using 50 μg/mL pDNA could better protect the pDNA compared to LNPs formulated with 100 μg/mL, as almost 90% of DNA was found intact vs 60%, respectively. However, cationic LNPs with 100 μg/mL preserved a larger amount of pDNA compared to 50 μg/mL LNPs, and the same protection was also detected after storage for 1 month. This specific formulation was thus tested in further in vitro toxicity and uptake studies.

Neutral LNPs loaded with 30–100 μg/mL pDNA were also tested for their protection ability against DNase I with the same protocol. Here, no significant differences were observed between the samples, with all LNPs preserving around 35% of the loaded pDNA intact after incubation with the enzyme (Figure 6C). Although the percentage of protected pDNA was lower compared to cationic LNPs, one-third of the fed pDNA could be protected, possibly loaded in the aqueous core of neutral LNPs during formulation in the microfluidic chip.

Toxicity and in vitro Behavior

Since cellular internalization of the LNPs is needed for a correct delivery of the cargo molecule, we evaluated whether cationic or neutral LNPs could be efficiently uptaken by ARPE-19 cells. ARPE-19 cells were chosen because an
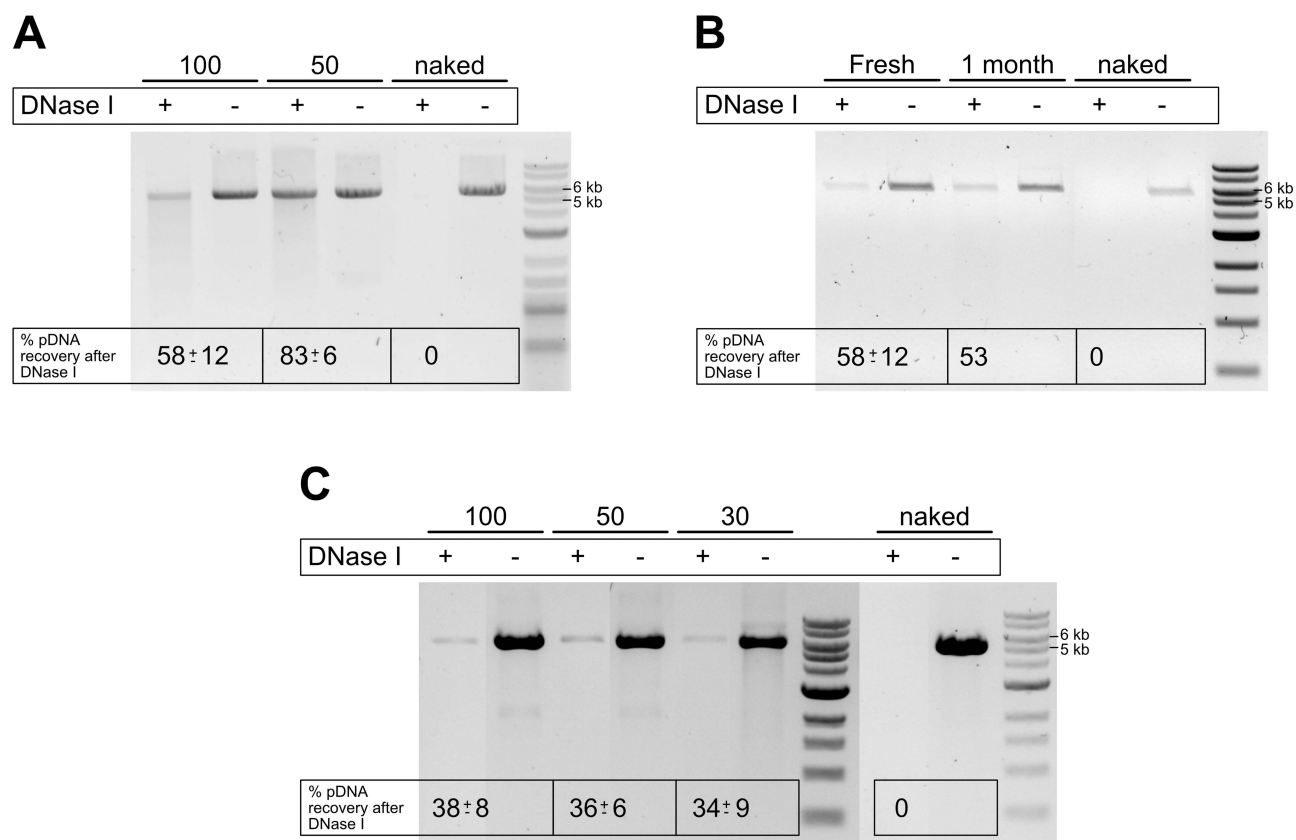
Figure 6 pDNA-LNPs protection of pDNA against DNase I. (**A**) Analysis by gel electrophoresis of DNA extracted from cationic pDNA-LNPs with 100 or 50 μg/mL DNA with or without pre-incubation with DNase I; (**B**) Analysis by gel electrophoresis of DNA extracted from cationic pDNA-LNPs with 100 μg/mL DNA as freshly formulated or after 1 month of storage, with or without pre-incubation with DNase I; (**C**) Analysis by gel electrophoresis of DNA extracted from neutral pDNA-LNPs with 100, 50, 30 μg/mL DNA with or without pre-incubation with DNase I. Below we reported as Mean ± SD the percentage of pDNA recovered after DNase I treatment compared to controls: untreated sample and unformulated naked pDNA.

approved AAV-based gene therapy (Luxturna) targets the retinal pigment epithelium of the eye of Leber congenital amaurosis patients. Secondly, in vivo the cells of the retinal pigment epithelium do not proliferate, limiting the dilution of the delivered DNA with time. We assessed intracellular uptake of LNPs at different time points by staining of the cells with Caveolin-1 and EEA1 (Early Endosome Antigen 1). We found that cationic LNPs were largely uptaken by the cells and that LNPs partially colocalized with Caveolin-1 and EEA1, especially at early time points (Figure 7A), suggesting that they might enter the cells through a caveolin-mediated endocytosis and transported to early endosomes. In comparison, we found that very few neutral LNPs entered the cells compared to the cationic ones, but they displayed a similar intracellular localization (Figure 7B). These data were confirmed by quantification of the red fluorescence of the labeled LNPs, and we found increasing mean fluorescence intensity with time, suggesting intracellular accumulation of cationic and neutral LNPs over time (Figure 7C).

In addition, to establish if exposure to LNPs could be toxic to the cells, ARPE-19 cells were incubated for 24 h with increasing concentrations of LNPs ranging from 4 to 400 μg/mL. Cationic LNPs showed a dose response with augmented toxicity at higher concentrations. Cationic LNPs also resulted more toxic than neutral LNPs, which decreased cell viability only about 10% (Figure 7D). In accordance, the same trend was observed after 48 h of exposure (Figure S4A). Nevertheless, none of the formulations resulted toxic at the lowest tested concentration, suggesting that cationic LNPs might still be suitable for in vivo applications.

Moreover, we tested toxicity of other formulations of both cationic and neutral LNPs and overall all formulations showed increased toxicity in a dose-dependent manner, with neutral LNPs impacting slightly less on cell viability then cationic LNPs, mainly after 24h (Figure S4B and C). The different outcomes of cationic and neutral LNPs on cell viability could be at least partially explained by the high intracellular accumulation of cationic LNPs, as described above,
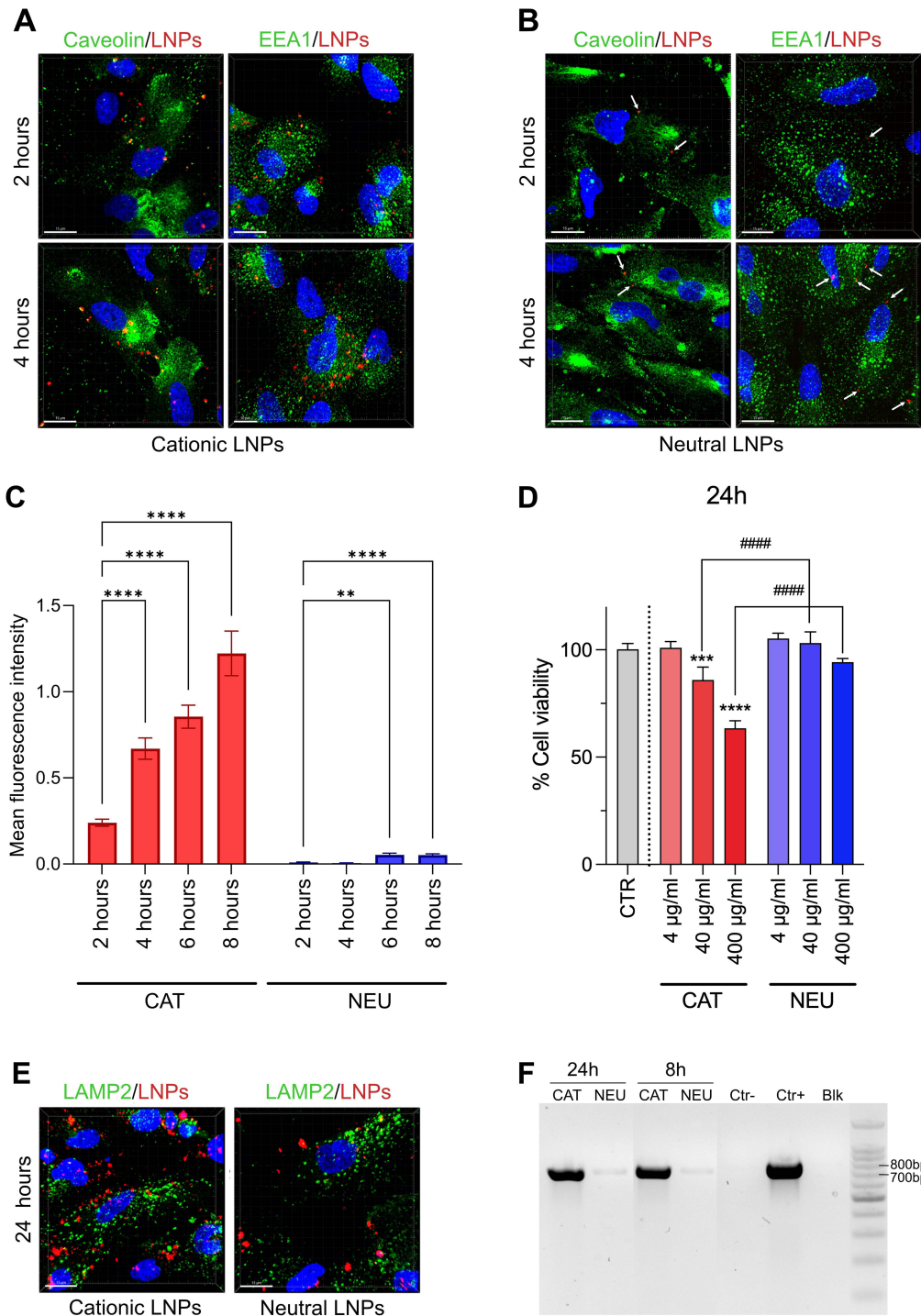
Figure 7 In vitro studies of cationic LNPs with 100 μg/mL DNA and neutral LNPs with 30 μg/mL DNA on ARPE-19 cells. Cellular internalization of cationic (**A**) and neutral (**B**) LPNs after 2 h and 4 h. Intracellular localization of LNPs (red) was assessed with Caveolin-1 and EEA1 staining (green) and nuclei of cells were stained with DAPI (blue). Arrows indicate neutral LNPs Scale bar: 15 μm. (**C**) Mean fluorescence intensity of intracellular LNPs over time. 10 fields with at least 100 cells were analyzed and data represented as Mean ± SD. (**D**) In vitro toxicity study. Cell viability assessed toxicity of cationic and neutral LNPs at 4, 40 and 400 μg/mL. Untreated cells were set at 100% cell viability and used as control. Asterisks represent significance compared to control, hashtags represent significance between the marked groups: **$p < 0.01$, ***$p < 0.001$, and ****or ####$p < 0.0001$. All data derive from three biological replicates and are shown as Mean ± SD. (**E**) Cellular internalization of cationic and neutral LPNs (red) after 24 h. Cellular lysosomes were identified with anti-LAMP2 (green) and nuclei of cells were stained with DAPI (blue). Scale bar: 15 μm. (**F**) PCR amplicons of a 728 bp region of the encapsulated pDNA. PCR was performed on the total DNA extracted from cells previously incubated 8 h or 24 h with LNPs. Cell culture wells without cells were used as negative control, to check for pDNA-LNPs unspecifically attached to the cell culture plate surface, and supernatants containing loaded LNPs were used as positive control.

and that is presumably higher at increasing LNP concentrations. In fact, we noticed that starting at around 6 h of incubation, uptaken LNPs formed aggregates that increased in number when more particles were present inside the cell, predominantly after 24 h of incubation (Figure 7E). Importantly, we found that most of the internalized particles did not colocalize with the lysosome marker LAMP2 (Lysosome Associated Membrane Protein 2), even after 24h of incubation (Figure 7E), hinting that the LNPs might be stable in the cytoplasm and do not undergo the degradation pathway mediated by lysosomes. LNPs had never been found inside the nucleus of treated cells.

To define whether pDNA-LNPs could allow expression from the delivered pDNA, we chose to assess expression of eGFP, that was encoded by the pDNA used for these experiments, in COS-7 cells that allow a prolonged expression of transfected DNA. eGFP expression mediated by cationic pDNA-LNPs was observed in COS-7 at 2 days and 5 days after exposure and expression increased with time, although in low amounts. Formulations stored for 1 month were still able to induce expression but with lower efficiency (Figure S5). We could not observe expression mediated by neutral DNA-LNPs in this set of experiments. The low efficiency in gene expression mediated by the formulated pDNA could be caused by degradation of the LNPs and pDNA if the early endosome fuse to lysosomes. To assess this hypothesis, total DNA was extracted from ARPE-19 cells incubated for 8 h or 24 h with pDNA-LNPs and pDNA was identified by PCR using specific primers that amplify a 728 bp region of the plasmid. An amplicon of the correct size could be detected in all samples, although for samples incubated with neutral LNPs the amount of DNA was very low, as expected by the low number of LNPs uptaken by the cells (Figure 7F). This assay proved that LNPs and pDNA are not degraded within 24 h inside the cell and confirmed that LNPs can protect the pDNA inside the cytoplasm.

Discussion

Recently, the use of microfluidics for the production of lipid nanoparticles for gene therapy has gained a lot of interest; however, every new formulation of LNPs must be optimized in composition and formulation protocol, analyzing their properties, stability, and efficacy. In this study, the aim was to use MF to formulate LNPs to deliver a plasmid DNA, by optimizing their lipid composition and productive strategy. Initial optimizations allowed us to fix the microfluidic parameters of FRR, TFR, lipid concentration, lipidic fraction, and composition of the aqueous phase, to produce monodisperse LNPs with a size around 150 nm that could be stable when stored at 4°C. Further optimization of the lipid fraction of the LNPs was required for DNA binding.[69,70] Therefore, we first optimized the amount of cationic lipid and fluorescent lipid to have small, monodispersed, cationic, fluorescent, stable LNPs.

Classical techniques to produce NPs for gene delivery include the formation of the cationic core structure, to which the DNA is added to form a complex by charge interaction (post-addition);[71–73] however, microfluidics offer innovative new possibilities for loading DNA in LNPs minimizing volumes while maximizing the interaction between the aqueous (DNA) and organic (lipidic) solvents. In a previous study, we demonstrated the importance of a liquid core to load hydrophilic molecules, like nucleic acids.[74] In this view, microfluidics offered two huge and unexpected advantages for the delivery of pDNA over the limited standard post-modification approach normally seen in the literature. First, the "pre" addition allowed to have almost 100% of pDNA bound to LNPs even with 100 μg/mL while maintaining their physical characteristics, which fall within the limits for good biodistribution and monodispersity, compared to the "pre" addition leading to poor NMed formation even at only 15 μg/mL, demonstrating how when this new technique is optimized could be incredibly advantageous for gene delivery. This might be even more effective for different types of carriers, such as polymeric or hybrids, where a "post-addition" method is still prevalent for gene delivery.

Secondly, it has been reported that the use of not only the microfluidic chips, but also different lipids, can induce a particular arrangement of the materials in the LNPs, resulting in a different interaction between the LNPs and the nucleic acids that might lead to varying in vitro and in vivo results between the two techniques.[75,76] Therefore, we propose that the standard dogma of cationic materials being necessary to load DNA (which is usually incompatible with negatively charged materials) may not apply. In fact, when the same microfluidic optimizations were applied to neutral DPPC:Chol LNPs, the NMeds demonstrated good efficiency in pDNA loading, incorporating up to 50% of the fed dose even without the cationic charge. While these LNPs did not bind 100% of the DNA, increasing the DNA amount in the formulation up to 100 μg/mL still, allows for drastically larger DNA loads than normally seen in the literature. This is also a major advantage because it removes one of the major adverse characteristics of cationic LNPs, which is the

permanent cationic charge due to the DOTAP that can cause cell toxicity in vitro and in vivo. This could pave the way for a different strategy from what has been published up to now, as the lack of cationic charge along with high DNA loading efficiency could produce, thanks to this production technique, efficient gene therapy tools without the toxicity generally associated with the cationic lipids. The major limitation that we found as expected in the use of neutral LNPs is that they were uptaken less compared to their cationic counterparts. This difference is widely reported in the literature, and it is due to a minor charge-based interactions of the neutral particles with proteins and receptors on the cell membrane;[77,78] however, we can overcome the limited uptake of the neutral particle by functionalizing the neutral particle with ligands for cell-specific delivery. This strategy, applied to LNPs that already showed reduced toxicity and high DNA loading might really represent a revolutionary step towards more safe, specific, and less toxic approaches for gene therapy.

It is important to note that phospholipids, as the ones used to produce these LNPs, are known to form dynamic structures that can continuously rearrange after interaction with a DNA molecule.[79–81] This is a critical point to discuss when considering a production protocol as the one here proposed, that should promote "encapsulation" of pDNA in the aqueous core of a lipidic vesicle. Unfortunately, given the dynamic nature of these objects, there is no evidence that the DNA is located in the core or adsorbed on the surface, or divided between the two locations in an equilibrium due to the possible flip-flop movement of the lipids.[82–84] Nonetheless, independent from the architecture of the resulting particle, it was paramount to assess the potential of both cationic and neutral LNPs to protect the bound pDNA from degradation. With a DNase I assay, we confirmed that the best performing cationic LNPs could protect almost 90% of the DNA. Interestingly, neutral LNPs could also protect around 35% of the pDNA used during the whole formulation. This fraction, compared to the amount of pDNA that these LNPs were able to retain in the band shift assay, means that almost 80% of the bound pDNA could be preserved. Although this is not an indication of the actual distribution of the pDNA molecules in the pDNA-LNP structure, data suggest that a major part of the genetic material is protected, either by encapsulation or steric hindrance and that neutral LNPs might be an efficient and non-toxic gene carrier, if properly optimized.

In vitro tests were performed to evaluate toxicity, intracellular biodistribution, and induction of expression of pDNA-LNPs. As expected, cationic LNPs appeared slightly more toxic compared to neutral LNPs, although both the formulations resulted not toxic at a concentration of 4 µg/mL. When analyzing the expression induction capacity in vitro, only a few cells were found to be GFP positive. As mentioned before, cationic LNPs were found to be uptaken more efficiently than neutral LNPs, as expected due to low interaction of neutral LNPs with the proteins at the cell membrane.[77,78] However, both cationic and neutral pDNA-LNPs were similarly internalized in early endosomes via caveolin-positive vesicles after 2h, and did not appear to fuse to lysosomes up to 24h. Moreover, the lack of induction efficacy was not correlated to the degradation of the DNA, as LNPs did not follow the lysosomal degradation pathway, and the pDNA was still intact when extracted. These data indicate that this formulation might be able to protect the genetic material in vivo in the cytoplasm, and that an efficient induction might be achieved with the surface modification of the LNPs with nuclear targeting peptides. This would maintain the positive properties of high loading and yield obtained with the "pre" strategy of the microfluidic technology, while also ensuring a higher nuclear localization of the DNA.

Overall, this study represents a first step towards the formulation of safe and efficient LNPs using the microfluidic technology, evidencing how this technology could revolutionize the way we are used to thinking about nanomedicine for gene therapy.

Conclusion

Gene therapy has become a leading research field for the treatment of diseases, but the application of nanomedicine to deliver the genetic material to the site of interest in a protected manner is no easy feat. Improving loading content and selecting the proper NMed material without compromising the protective nature of the system is critical. These results were able to combine microfluidic scaling with improved loading, protection, and stability of pDNA in neutral LNPs, paving the way for more advanced studies in vitro and in vivo for advanced gene therapy applications.

Funding

Disclosure

The authors report no conflicts of interest in this work.

References

1. Wu L-P, Wang D, Li Z. Grand challenges in nanomedicine. *Mater Sci Eng C*. 2020;106:110302. doi:10.1016/j.msec.2019.110302
2. Shi Y. Clinical translation of nanomedicine and biomaterials for cancer immunotherapy: progress and perspectives. *Adv Ther*. 2020;3:1900215. doi:10.1002/adtp.201900215
3. Zhang C, Yan L, Wang X, et al. Progress, challenges, and future of nanomedicine. *Nano Today*. 2020;35:101008. doi:10.1016/j.nantod.2020.101008
4. Pederzoli F, Ruozi B, Duskey J. Nanomedicine Against Aβ aggregation by β–sheet breaker peptide delivery: in vitro evidence. *Pharmaceutics*. 2019;11(11):572. doi:10.3390/pharmaceutics11110572
5. Oddone N, Boury F, Garcion E, et al. Synthesis, characterization, and in vitro studies of an reactive oxygen species (ROS)-responsive methoxy polyethylene glycol-thioketal-melphalan prodrug for glioblastoma treatment. *Front Pharmacol*. 2020;11. doi:10.3389/fphar.2020.00574
6. Ottonelli I, Bighinati A, Adani E, et al. Optimization of an injectable hydrogel depot system for the controlled release of retinal-targeted hybrid nanoparticles. *Pharmaceutics*. 2023;15:25. doi:10.3390/pharmaceutics15010025
7. Faouzi A, Roullin VG. Think big, start small: how nanomedicine could alleviate the burden of rare CNS diseases. *Pharmaceuticals*. 2021;14:109. doi:10.3390/ph14020109
8. Dash SR, Kundu CN. Advances in nanomedicine for the treatment of infectious diseases caused by viruses. *Biomater Sci*. 2023;11:3431–3449. doi:10.1039/D2BM02066A
9. Feng L, Wang H, Xue X. Recent progress of nanomedicine in the treatment of central nervous system diseases. *Adv Ther*. 2020;3:1900159. doi:10.1002/adtp.201900159
10. Cano A, Turowski P, Ettcheto M, et al. Nanomedicine-based technologies and novel biomarkers for the diagnosis and treatment of Alzheimer's disease: from current to future challenges. *J Nanobiotechnol*. 2021;19:122. doi:10.1186/s12951-021-00864-x
11. Tewabe A, Abate A, Tamrie M, Seyfu A, Abdela Siraj E. Targeted drug delivery — from magic bullet to nanomedicine: principles, challenges, and future perspectives. *J Multidiscip Healthc*. 2021;14:1711–1724. doi:10.2147/JMDH.S313968
12. Duskey JT, Rinaldi A, Ottonelli I, et al. Glioblastoma multiforme selective nanomedicines for improved anti-cancer treatments. *Pharmaceutics*. 2022;14:1450. doi:10.3390/pharmaceutics14071450
13. Li Q, Zhou Y, He W, et al. Platelet-armored nanoplatform to harmonize janus-faced IFN-γ against tumor recurrence and metastasis. *J Control Release*. 2021;338:33–45. doi:10.1016/j.jconrel.2021.08.020
14. Shen H, Huang X, Min J, et al. Nanoparticle Delivery Systems for DNA/RNA and their Potential Applications in Nanomedicine. *CTMC*. 2019;19:2507–2523. doi:10.2174/1568026619666191024170212
15. Zhan Y, Ma W, Zhang Y, et al. DNA-based nanomedicine with targeting and enhancement of therapeutic efficacy of breast cancer cells. *ACS Appl Mater Interfaces*. 2019;11:15354–15365. doi:10.1021/acsami.9b03449
16. Azeem F. Nanomedicine and gene delivery. In: *Nanomedicine Manufacturing and Applications*. Elsevier; 2021:247–260. doi:10.1016/B978-0-12-820773-4.00007-X
17. Chen Q, Sun T, Jiang C. Recent advancements in nanomedicine for 'cold' tumor immunotherapy. *Nano-Micro Lett*. 2021;13:92.
18. Kim S, Thuy LT, Lee J, Choi JS. Second-generation polyamidoamine dendrimer conjugated with oligopeptides can enhance plasmid DNA delivery in vitro. *Molecules*. 2023;28:7644. doi:10.3390/molecules28227644
19. Lee J, Kwon Y-E, Edwards SD, Guim H, Jae Jeong K. Improved biocompatibility of dendrimer-based gene delivery by histidine-modified nuclear localization signals. *Int J Pharm*. 2023;644:123299. doi:10.1016/j.ijpharm.2023.123299
20. Saviano F, Lovato T, Russo A, et al. Ornithine-derived oligomers and dendrimers for in vitro delivery of DNA and ex vivo transfection of skin cells via saRNA. *J Mater Chem B*. 2020;8:4940–4949. doi:10.1039/D0TB00942C
21. Lu C, Li Z, Chang L, et al. Efficient Delivery of dsRNA and DNA in cultured silkworm cells for gene function analysis using PAMAM dendrimers system. *Insects*. 2019;11:12. doi:10.3390/insects11010012
22. Kisakova LA, Apartsin EK, Nizolenko LF, Karpenko LI. Dendrimer-Mediated Delivery of DNA and RNA Vaccines. *Pharmaceutics*. 2023;15:1106. doi:10.3390/pharmaceutics15041106
23. Trigueros SB, Domènech E, Toulis V, Marfany G. In vitro gene delivery in retinal pigment epithelium cells by plasmid DNA-wrapped gold nanoparticles. *Genes*. 2019;10:289. doi:10.3390/genes10040289
24. Siddique S, Chow JCL. Gold nanoparticles for drug delivery and cancer therapy. *Appl Sci*. 2020;10:3824. doi:10.3390/app10113824
25. Ramírez-Acosta CM, Cifuentes J, Castellanos MC, et al. PH-responsive, cell-penetrating, core/shell magnetite/silver nanoparticles for the delivery of plasmids: preparation, characterization, and preliminary in vitro evaluation. *Pharmaceutics*. 2020;12:561. doi:10.3390/pharmaceutics12060561

26. Karimov M, Scherer M, Franke H, Ewe A, Aigner A. Analysis of polymeric nanoparticle properties for siRNA/DNA delivery in a tumor xenograft tissue slice air–liquid interface model. *Biotechnol J*. 2023;18:2200415. doi:10.1002/biot.202200415

27. Dilliard SA, Siegwart DJ, Moore A, Coreas R. Passive, active and endogenous organ-targeted lipid and polymer nanoparticles for delivery of genetic drugs. *Nat Rev Mater*. 2023;1–19. doi:10.1038/s41578-022-00529-7

28. Marwaha MG, Awasthi R, Marwaha RK, et al. Emerging applications of polymeric nanoparticles in tumor targeting. *CNANO*. 2023;19:677–696. doi:10.2174/1573413718666220928114233

29. Shen X, Dirisala A, Toyoda M, et al. pH-responsive polyzwitterion covered nanocarriers for DNA delivery. *J Control Release*. 2023;360:928–939. doi:10.1016/j.jconrel.2023.07.038

30. Baumhover NJ, Duskey JT, Khargharia S, et al. Structure–activity relationship of pegylated polylysine peptides as scavenger receptor inhibitors for non-viral gene delivery. *Mol Pharm*. 2015;12:4321–4328. doi:10.1021/acs.molpharmaceut.5b00513

31. Vaughan HJ, Zamboni CG, Hassan LF, et al. Polymeric nanoparticles for dual-targeted theranostic gene delivery to hepatocellular carcinoma. *Sci Adv*. 2022;8:eabo6406. doi:10.1126/sciadv.abo6406

32. Liu GW, Guzman EB, Menon N, Langer RS. Lipid nanoparticles for nucleic acid delivery to endothelial cells. *Pharm Res*. 2023;40:3–25. doi:10.1007/s11095-023-03471-7

33. Pardridge WM. Brain gene therapy with Trojan horse lipid nanoparticles. *Trends Mol Med*. 2023;29:343–353. doi:10.1016/j.molmed.2023.02.004

34. Wei X, Li Y, Cheng X, et al. Increase nebulization stability of lipid nanoparticles by integrating a DNA supramolecular hydrogel. *ACS Macro Lett*. 2023;12:745–750. doi:10.1021/acsmacrolett.3c00183

35. Pfeifle A, Thulasi raman SN, Lansdell C, et al. DNA lipid nanoparticle vaccine targeting outer surface protein C affords protection against homologous Borrelia burgdorferi needle challenge in mice. *Front Immunol*. 2023;14:1020134. doi:10.3389/fimmu.2023.1020134

36. Zhu Y, Shen R, Vuong I, et al. Multi-step screening of DNA/lipid nanoparticles and co-delivery with siRNA to enhance and prolong gene expression. *Nat Commun*. 2022;13:4282. doi:10.1038/s41467-022-31993-y

37. Jiang T, Gonzalez KM, Cordova LE, Lu J. Nanotechnology-enabled gene delivery for cancer and other genetic diseases. *Expert Opin Drug Delivery*. 2023;20:523–540. doi:10.1080/17425247.2023.2200246

38. Vaughan HJ, Zamboni CG, Luly KM, et al. Non-viral gene delivery to hepatocellular carcinoma via intra-arterial injection. *IJN*. 2023;18:2525–2537. doi:10.2147/IJN.S390384

39. Wang C, Pan C, Yong H, et al. Emerging non-viral vectors for gene delivery. *J Nanobiotechnol*. 2023;21:272. doi:10.1186/s12951-023-02044-5

40. Sun D, Lu Z-R. Structure and function of cationic and ionizable lipids for nucleic acid delivery. *Pharm Res*. 2023;40:27–46. doi:10.1007/s11095-022-03460-2

41. Jahanafrooz Z, Baradaran B, Mosafer J, et al. Comparison of DNA and mRNA vaccines against cancer. *Drug Discov Today*. 2020;25:552–560. doi:10.1016/j.drudis.2019.12.003

42. Kimura S, Khalil IA, Elewa YHA, Harashima H. Novel lipid combination for delivery of plasmid DNA to immune cells in the spleen. *J Control Release*. 2021;330:753–764. doi:10.1016/j.jconrel.2021.01.005

43. Begagić E, Bečulić H, Đuzić N, et al. CRISPR/Cas9-mediated gene therapy for glioblastoma: a scoping review. *Biomedicines*. 2024;12:238. doi:10.3390/biomedicines12010238

44. Lampe GD, King RT, Halpin-Healy TS, et al. Targeted DNA integration in human cells without double-strand breaks using CRISPR-associated transposases. *Nat Biotechnol*. 2024;42:87–98. doi:10.1038/s41587-023-01748-1

45. Webber BR. Cas9-induced targeted integration of large DNA payloads in primary human T cells via homology-mediated end-joining DNA repair. *Nat Biomed Eng*. 2023;1–18. doi:10.1038/s41551-023-01157-4

46. Tao J, Bauer DE, Chiarle R. Assessing and advancing the safety of CRISPR-Cas tools: from DNA to RNA editing. *Nat Commun*. 2023;14:212. doi:10.1038/s41467-023-35886-6

47. Sinclair F, Begum AA, Dai CC, Toth I, Moyle PM. Recent advances in the delivery and applications of nonviral CRISPR/Cas9 gene editing. *Drug Deliv Transl Res*. 2023;13:1500–1519. doi:10.1007/s13346-023-01320-z

48. Maeki M, Okada Y, Uno S, et al. Mass production system for RNA-loaded lipid nanoparticles using piling up microfluidic devices. *Appl Mater Today*. 2023;31:101754. doi:10.1016/j.apmt.2023.101754

49. Lin Z, Zou Z, Pu Z, Wu M, Zhang Y. Application of microfluidic technologies on COVID-19 diagnosis and drug discovery. *Acta Pharmaceutica Sinica B*. 2023;13:2877–2896. doi:10.1016/j.apsb.2023.02.014

50. Tarim EA, Anil Inevi M, Ozkan I, et al. Microfluidic-based technologies for diagnosis, prevention, and treatment of COVID-19: recent advances and future directions. *Biomed Microdevices*. 2023;25:10. doi:10.1007/s10544-023-00649-z

51. Huang Y, Liu C, Feng Q, Sun J. Microfluidic synthesis of nanomaterials for biomedical applications. *Nanoscale Horiz*. 2023;8:1610–1627. doi:10.1039/D3NH00217A

52. Ejeta F. Recent advances of microfluidic platforms for controlled drug delivery in nanomedicine. *DDDT*. 2021;15:3881–3891. doi:10.2147/DDDT.S324580

53. Matsuura-Sawada Y, Maeki M, Nishioka T, et al. Microfluidic device-enabled mass production of lipid-based nanoparticles for applications in nanomedicine and cosmetics. *ACS Appl Nano Mater*. 2022;5:7867–7876. doi:10.1021/acsanm.2c00886

54. Boyd BJ, McDowell A. Microfluidics in Nanomedicine. *PNT*. 2019;7:422. doi:10.2174/2211738507061912100152137

55. Jaradat E, Weaver E, Meziane A, Lamprou DA. Microfluidics Technology for the Design and Formulation of Nanomedicines. *Nanomaterials*. 2021;11:3440. doi:10.3390/nano11123440

56. Prakash G, Shokr A, Willemen N, et al. Microfluidic fabrication of lipid nanoparticles for the delivery of nucleic acids. *Adv Drug Delivery Rev*. 2022;184:114197. doi:10.1016/j.addr.2022.114197

57. Chiesa E, Bellotti M, Caimi A, et al. Development and optimization of microfluidic assisted manufacturing process to produce PLGA nanoparticles. *Int J Pharm*. 2022;629:122368. doi:10.1016/j.ijpharm.2022.122368

58. Tomeh MA, Mansor MH, Hadianamrei R, Sun W, Zhao X. Optimization of large-scale manufacturing of biopolymeric and lipid nanoparticles using microfluidic swirl mixers. *Int J Pharm*. 2022;620:121762. doi:10.1016/j.ijpharm.2022.121762

59. Gimondi S, Ferreira H, Reis RL, Neves NM. Microfluidic devices: a tool for nanoparticle synthesis and performance evaluation. *ACS Nano*. 2023;17:14205–14228. doi:10.1021/acsnano.3c01117

60. Hermosilla J, Alonso-García A, Salmerón-García A, et al. Analysing the In-Use Stability of mRNA-LNP COVID-19 vaccines comirnaty™ (Pfizer) and Spikevax™ (Moderna): a comparative study of the particulate. *Vaccines*. 2023;11:1635. doi:10.3390/vaccines11111635

61. Ottonelli I, Duskey JT, Rinaldi A, et al. Microfluidic Technology for the Production of Hybrid Nanomedicines. *Pharmaceutics*. 2021;13:1495. doi:10.3390/pharmaceutics13091495

62. Laramy O, N. M, Cebrero YM, et al. Process robustness in lipid nanoparticle production: a comparison of microfluidic and turbulent jet mixing. *Mol Pharm*. 2023;20:4285–4296. doi:10.1021/acs.molpharmaceut.3c00390

63. Tiboni M, Tiboni M, Pierro A, et al. Microfluidics for nanomedicines manufacturing: an affordable and low-cost 3D printing approach. *Int J Pharm*. 2021;599:120464. doi:10.1016/j.ijpharm.2021.120464

64. Khorshid S, Montanari M, Benedetti S, et al. A microfluidic approach to fabricate sucrose decorated liposomes with increased uptake in breast cancer cells. *Eur J Pharm Biopharm*. 2022;178:53–64. doi:10.1016/j.ejpb.2022.07.015

65. Dunn KC, Aotaki-Keen AE, Putkey FR, Hjelmeland LM. ARPE-19, a human retinal pigment epithelial cell line with differentiated properties. *Exp Eye Res*. 1996;62:155–169. doi:10.1006/exer.1996.0020

66. Ruozi B, Tosi G, Leo E, Vandelli MA. Application of atomic force microscopy to characterize liposomes as drug and gene carriers. *Talanta*. 2007;73:12–22. doi:10.1016/j.talanta.2007.03.031

67. Ruozi B, Belletti D, Tombesi A, et al. AFM, ESEM, TEM, and CLSM in liposomal characterization: a comparative study. *Int j Nanomed*. 2011;6:557–563. doi:10.2147/IJN.S14615

68. Ruozi B, Tosi G, Forni F, Fresta M, Vandelli MA. Atomic force microscopy and photon correlation spectroscopy: two techniques for rapid characterization of liposomes. *Eur J Pharm Sci*. 2005;25:81–89. doi:10.1016/j.ejps.2005.01.020

69. Sinegra AJ, Evangelopoulos M, Park J, Huang Z, Mirkin CA. Lipid nanoparticle spherical nucleic acids for intracellular DNA and RNA delivery. *Nano Lett*. 2021;21:6584–6591. doi:10.1021/acs.nanolett.1c01973

70. Hald Albertsen C, Kulkarni JA, Witzigmann D, et al. The role of lipid components in lipid nanoparticles for vaccines and gene therapy. *Adv Drug Delivery Rev*. 2022;188:114416. doi:10.1016/j.addr.2022.114416

71. Caracciolo G, Amenitsch H. Cationic liposome/DNA complexes: from structure to interactions with cellular membranes. *Eur Biophys J*. 2012;41:815–829. doi:10.1007/s00249-012-0830-8

72. Levine RM, Pearce TR, Adil M, Kokkoli E. Preparation and characterization of liposome-encapsulated plasmid DNA for gene delivery. *Langmuir*. 2013;29:9208–9215. doi:10.1021/la400859e

73. Lopez A, Liu J. DNA oligonucleotide-functionalized liposomes: bioconjugate chemistry, biointerfaces, and applications. *Langmuir*. 2018;34:15000–15013. doi:10.1021/acs.langmuir.8b01368

74. Huang L, Himawan E, Belhadj S, et al. Efficient delivery of hydrophilic small molecules to retinal cell lines using gel core-containing solid lipid nanoparticles. *Pharmaceutics*. 2021;14:74. doi:10.3390/pharmaceutics14010074

75. Gilbert J, Ermilova I, Fornasier M, et al. On the interactions between RNA and titrateable lipid layers: implications for RNA delivery with lipid nanoparticles. *Nanoscale*. 2024;16:777–794. doi:10.1039/D3NR03308B

76. Kloczewiak M, Banks JM, Jin L, Brader ML. A biopharmaceutical perspective on higher-order structure and thermal stability of mRNA vaccines. *Mol Pharm*. 2022;19:2022–2031. doi:10.1021/acs.molpharmaceut.2c00092

77. Fröhlich E. The role of surface charge in cellular uptake and cytotoxicity of medical nanoparticles. *Int j Nanomed*. 2012;7:5577–5591. doi:10.2147/IJN.S36111

78. Salatin S, Maleki Dizaj S, Yari Khosroushahi A. Effect of the surface modification, size, and shape on cellular uptake of nanoparticles. *Cell Biol Int*. 2015;39:881–890. doi:10.1002/cbin.10459

79. Ma B, Zhang S, Jiang H, Zhao B, Lv H. Lipoplex morphologies and their influences on transfection efficiency in gene delivery. *J Control Release*. 2007;123:184–194. doi:10.1016/j.jconrel.2007.08.022

80. Gupta S, De Mel JU, Schneider GJ. Dynamics of liposomes in the fluid phase. *Curr Opin Colloid Interface Sci*. 2019;42:121–136. doi:10.1016/j.cocis.2019.05.003

81. Schoenmaker L, Witzigmann D, Kulkarni JA, et al. mRNA-lipid nanoparticle COVID-19 vaccines: structure and stability. *Int J Pharm*. 2021;601:120586. doi:10.1016/j.ijpharm.2021.120586

82. Gu R-X, Baoukina S, Tieleman DP. Cholesterol Flip-Flop in Heterogeneous Membranes. *J Chem Theory Comput*. 2019;15:2064–2070. doi:10.1021/acs.jctc.8b00933

83. Gurtovenko AA, Vattulainen I. Molecular mechanism for lipid flip-flops. *J Phys Chem B*. 2007;111:13554–13559. doi:10.1021/jp077094k

84. Nguyen MHL, DiPasquale M, Rickeard BW, et al. Peptide-induced lipid flip-flop in asymmetric liposomes measured by small angle neutron scattering. *Langmuir*. 2019;35:11735–11744. doi:10.1021/acs.langmuir.9b01625